Click to view slides of presentation.

4D Finite Difference Forward Modeling within a Redefined Closed-Loop Seismic Reservoir Monitoring Workflow*

David Hill[1,2], Dominic Lowden[1], Sonika[1], and Chris Koeninger[1]

Search and Discovery Article #41922 (2016)**
Posted November 7, 2016

*Adapted from extended abstract prepared in relation to oral presentation, and from presentation itself, given at GEO 2016, 12th Middle East Geosciences Conference & Exhibition, Manama, Bahrain, March 7-10, 2016

[1]Schlumberger, Houston, Texas (CKoeninger@slb.com)
[2]Currentlyconsultant/advisor, Redhill, UK

Abstract

Chimera is used to illustrate, in detail, the full-field 4D image-modeling workflow. The results of a Sim-to-Seis workflow are presented first, followed by the results from the full-field 4D image-modeling workflow, and the resultant predicted 4D-responses are compared. As Sim-to-Seis workflows do not address any geomechanical effects, and to ensure a valid comparison with the redefined forward modeling workflow, the material presented focuses on the reservoir. The geomechanics will be included in a later publication.

One component of the redefined closed-loop seismic reservoir monitoring workflow is Full- Field 4D Image-Modeling. Full-field 4D image-modeling incorporates the geologic, reservoir simulation, and reservoir geomechanical models into an integrated full-field coupled dynamic integrated earth model to surface. From which 3D grids of petro-elastic parameters for a range of reservoir simulations are derived via the rock-physics model for input into finite-difference forward-modeling and imaging. By including 3D wave propagation, acquisition geometry, overburden illumination, near surface effects and calibrated noise the seismically measurable 4D-response predicted via full-field 4D image-modeling is more robust, and of a higher fidelity than is achievable via the more traditional Sim-to-Seis type workflows.

Full-Field 4D Image-Modeling workflow:

- Integrates the reservoir, geologic and geomechanical models into a dynamic integrated earth model. compaction and subsidence to surface can be modeled into future time for a range of production scenarios.
- Noise free forward-modeling provides a qualitative understanding of the nature, magnitude and distribution of the 4D-response into future time and ties reservoir changes to the corresponding seismically measurable 4D-response.

- With the inclusion of calibrated noise the forward-modeling models the seismically measurable 4D-response, from which the optimal measurement method and acquisition design can be determined; so as to record the seismically measurable 4D-response at the required time-steps for proactive seismic reservoir monitoring.
- Moreover, with the advent of modern computer architectures the elapsed time for the full-field 4D image-modeling is measured in single digit months.

Full-Field 4D Image-Modeling is necessary to fully understand the complexities of reservoir property changes over time, to assess whether those changes are seismically detectable and to make informed decisions on the 4D time-lapse measurement method, design, and reservoir monitoring strategy. Such an in depth understanding cannot be achieved using one of the more traditional Sim-to-Seis type workflows.

Introduction

The history of closed-loop seismic reservoir monitoring (CL-SRM) dates back to the late 1990s to early 2000s. In the paper "History Matching Using Time-Lapse Seismic (HUTS)" (Gosselin et al., 2003), the authors noted that at the time the seismic forward-modeling step within the proposed workflow was too "cpu-time consuming". Hence they confined themselves to "closing the loop" by reconciling the differences between elastic parameter changes, predicted from reservoir simulations, with measured elastic parameter changes from an acoustic impedance inversion of 4D time-lapse seismic data. In the subsequent years variations of the HUTS CL-SRM workflow were developed and generically assigned the descriptors "Sim-to-Seis" and Seis-to-Sim" workflows, illustrated in Figure 1.

Within these workflows, various forward-modeling techniques to generate synthetic seismic data evolved in line with the availability of computing resources. Three groups of forward-modeling techniques currently in common use are: 1) direct analytical transformation of reservoir properties to seismic acoustic attributes, and variations of well-log-based fluid-substitution and petrophysical modeling, 2) 1D convolution modeling and 3) 2D/3D point spread function convolutional modeling (Lecomte, 2004). The first two modeling techniques neglect effects due to 3D wave propagation, acquisition geometry, overburden illumination, near surface and noise. While the third incorporates effects due to acquisition geometry and overburden illumination via ray-tracing, but it still neglects effects due to 3D wave propagation, near surface and noise. In many cases, the study area for such a Sim-to-Seis workflow has a small areal extent and is often confined to the reservoir interval. Moreover, the assumptions inherent in a Sim-to-Seis workflow deliver a forward model which is not necessarily a realistic representation of the measured 4D seismic response, and therefore renders it difficult or impossible to reconcile the differences and close the loop.

Recent advances in computer architecture have negated the premise that the seismic forward-modeling is too "cpu-time consuming". Large-scale 3D finite-difference acoustic and elastic modeling and imaging now permit accurate modeling of seismic data, where the modeling incorporates effects due to specific acquisition geometries, 3D wave-propagation, near-surface heterogeneities, overburden illumination, and representative random and residual coherent noise models etc. Hence, finite-difference modeling and imaging enables a robust prediction of a seismically measurable 4D response when provided with the appropriate 3D petro-elastic property models of Vp, Vs, density and anisotropic parameters as a function of each 4D time-step.

In parallel, research increasingly indicated the 4D-response associated with production was not restricted to the reservoir, but propagates into the overburden, side-burden, and under-burden driven by geomechanical effects. Consequently, to make a robust prediction of the 4D-response related to production, field-scale modeling has to incorporate the acoustic and elastic response to both reservoir and field-wide changes. This complex interaction incorporates the reservoir dynamics component - which encompasses fluid properties, fluid flow characteristics, field performance history and pressure distributions and profiles over time and the changes in stress induced by the pressure changes during production. These stress changes induce strains and deformations not only within the reservoir but also around it. Understanding the complete reservoir dynamics is not possible from studying the individual geological, static and dynamic reservoir, and geomechanical models in isolation – it requires they be integrated into a full-field coupled Dynamic Integrated Earth Model (DIEM), so they can be analyzed as a single integrated model.

The combination of a DIEM and finite-difference modeling and imaging has allowed a redefinition of the HUTS CL-SRM workflow (Figure 2). The redefined workflow models the three dimensional 4D-response as a function of all subsurface effects due to hydrocarbon production and incorporating effects due to acquisition configuration, overburden illumination and survey specific coherent and random noise.

The workflow described in Figure 2 is a two-pass process. The first pass (Full-Field 4D Image-Modeling) starts from the DIEM and passes through a rock-physics model to generate 3D petro-elastic property models of Vp, Vs, density and anisotropic parameters to surface for simulated reservoir changes as a function of 4D time-step. The 3D petro-elastic property models drive the finite-difference modeling and imaging steps, and the resultant images are differenced to derive the corresponding 4D-response. The sensitivity of the 4D-response is analyzed to assess its nature, magnitude, and distribution, the frequency of 4D time-lapse monitoring and the associated base-line and monitor acquisition method and design. Assuming a detectable 4D-response, the second pass starts from the processed 4D time-lapse seismic and progresses through the inverse process to the reservoir simulation.

The value of a robust full-field 4D image-modeling study as a component in a CL-SRM workflow are maximized when forward-modeled base-line 3D data are compared with, and calibrated to, the extant measured base-line 3D data, and then used to assist with static-model reconciliation (Ullman de Brito, 2011, Nur Rabani, 2014). Subsequently the forward-modeled 4D data (to the monitor date or dates) are compared with the extant 4D monitor data to assist with dynamic-model reconciliation (Nur Rabani, 2014). Comparing high fidelity forward-modeled 3D and 4D time-lapse seismic data with the corresponding optimally processed recorded seismic data offers detailed insight into coupled reservoir fluid flow and geomechanical processes, facilitating and update and calibration of the DIEM. (Taggart, 2008, Hurren, 2012, Pluchery, 2013).

Chimera DIEM

A synthetic oilfield model, called Chimera, has been constructed for Life of Field modeling. The Chimera DIEM (Figure 3) has within it a turbidite type reservoir with a maximum sand porosity of 25% and a maximum permeability of 200 mD. Hydrocarbons accumulate within a 4-way structural trap segmented by normal faults. The reservoir contains light oil supported by an aquifer from below and is associated with an initial gas cap. The DIEM dimensions are 25km x 25 km and 4km deep and contain 28 million cells, with 6.4 million cells in the reservoir interval. The simulated production scenario is primary depletion, followed by water injection. The simulated production begins at a 2014 base-

line date and progresses through to 2038 with properties output at 3-year increments. The top reservoir is at a depth of 1864m, the gas-oil interface at 1975m, and the oil-water interface at 2250m

This article will use Chimera to illustrate in detail the full-field 4D image-modeling workflow of the 1st pass (left column Figure 2). The results of a Sim-to-Seis workflow will be presented first, followed by the results from the full-field 4D image-modeling workflow, and the resultant predicted 4D-responses compared. As Sim-to-Seis workflows do not address any geomechanical effects, in order to ensure a valid comparison with the redefined forward-modeling workflow, the material presented here will focus on the reservoir, and geomechanics will be included in a later publication.

Sim-to-Seis Seismic Attribute Modeling

In their simplest form Sim-to-Seis and well-log-based fluid-substitution workflows are an analytical transformation of reservoir properties into seismic attributes via a rock-physics model. This type of workflow does not necessarily incorporate a representative wavelet and neglects effects due to 3D wave propagation, acquisition configuration, near surface and overburden illumination and noise. Reflectivity-based 1D convolutional modeling incorporates a representative wavelet and neglects the same list of effects. Reflectivity based 2D and 3D convolutional Point Spread Function Modeling (Lecomte, 2004) incorporates a representative wavelet and effects due to acquisition configuration and overburden illumination via ray-tracing but neglects effects due to 3D wave propagation, near surface and noise. In many cases the study area for a Sim-to-Seis workflow has a small areal extent and is often confined to the reservoir interval. As 3D convolutional point spread function modeling is one of the more sophisticated Sim-to-Seis workflows currently in common use, the results from this workflow using Chimera will be used for comparison with full-field 4D image-modeling.

Figure 4 depicts a vertical section through reflectivity cubes, generated from the Chimera velocity and density cubes, convolved with 3D point spread functions characterized by a 30hz Ricker wavelet for 2014 and 2017. Figure 5 shows the point spread function 4D time-lapse differences for 2017 to 2014, 2020 to 2014, 2026 to 2014 and 2038 to 2014, with pairs of arrows for the gas-oil and oil-water interfaces, one of which is annotated with a Δ to highlight the fluid front movement through these periods.

Figure 5 clearly illustrates the fluid movements for the gas-oil and oil-water interfaces for these time-steps but does not demonstrate whether these fluid movements will be seismically detectable. As Sim-to-Seis workflows do not generate non-zero-offset pre-stack seismic-like gathers, incorporating realistic noise models derived from real seismic data is a non-trivial task. Therefore, where noise is added to a Sim-to-Seis workflow, it is often limited to just random noise, where the random noise are scaled to simulate a range of signal to noise ratios without any mechanism to accurately calibrate to real seismic data. Hence, a Sim-to-Seis workflow with the inclusion of random noise will only allow a qualitative decision on the seismic detectability of the 4D-response.

Full-Field 4D Image-Modeling

Historic literature showed that the measured 4D-response often mismatched the predicted response (Calvert, 2005; Johnston, 2013). This mismatch may be attributable to either an inaccurate rock-physics model, or an insufficiently sophisticated approach to the forward-modeling

of the predicted 4D-response by not taking the full subsurface changes into account, or a combination of both. Accurate rock-physics transfer functions that adequately translate the production scenarios to petro-elastic properties are fundamental to the accuracy of the predicted 4D seismic response (Ullman de Brito, 2011).

A full-field 4D image-modeling study should deliver a robust and reliable prediction of the 4D-response, with associated uncertainties, as well as the optimal acquisition design, necessary to measure the 4D-response at the required time interval for proactive reservoir management. Failure to do so may compromise the reservoir management strategy via a recorded 4D response with an inadequate signal-to-noise ratio, missed 4D opportunities, or sub-optimal repeat survey timings.

Given the focus here is on the reservoir alone, the relevant considerations in a full-field 4D image-modeling study are:

1. Determine the range of uncertainties and unknowns in the reservoir model.
2. Determine the range of uncertainties and unknowns in the rock-physics model.
3. Determine the production strategy to be simulated: Primary, IOR (Water, Gas, WAG) EOR (Chemical, Polymer) etc. over what time 4D time-steps.
4. Quantify the nature, magnitude and distribution of the measurable 4D-response associated uncertainties.
5. Determine the measurement method with highest probability of measuring the 4D response at the required time-step for proactive reservoir management: Surface seismic, 3D VSP, X-Well, EM, etc. and the associated measurement method configuration: source and receiver sampling etc.

The full-field 4D image-modeling workflow, illustrated in Figure 6, addresses the above considerations.

Ancillary Modeling Parameters

Before embarking upon finite-difference modeling with the derived 3D petro-elastic property models, ancillary modeling parameters are determined via the more traditional methods of convolutional modeling, 1D elastic modeling, ray trace modeling, and wedge modeling. Finite-difference compute costs scale with increased frequency; consequently, it is necessary to determine the maximum modeling frequency required to meet the geophysical objectives. Plotted in Figure 7 is the apparent amplitude spectra for the base-line 5085 cu in source array as a function of two-way travel-time, modeled incorporating absorption with a Q value of 150; derived from the base-line data. With an estimate of the noise floor in dB; annotated with the horizontal dashed red line, plus knowledge of the target two-way travel-time, the maximum recordable frequency at the target depth can be determined; annotated with the vertical red arrow. The maximum recordable frequency therefore becomes the maximum frequency modeled in the finite-difference modeling.

In addition to the ancillary modeling parameters, a master acquisition geometry and representative noise models are required. The master acquisition geometry (Table 1) is a super-set of the base-line geometry and is decimated back to the base-line geometry and multiple other geometries of interest in order to determine which acquisition geometry will measure the 4D-response at the required time interval.

To build field specific noise models the measured base-line seismic data, fully processed to the pre-stack imaging step, are decomposed prior to imaging into: measured seismic signal, measured residual coherent noise and measured random noise (Figure 8). The measured residual coherent noise and random noise are sorted to shot gathers to form the basic shot-domain noise models, which are then scaled appropriately and summed with the finite-difference modeled base-line shot gather (Figure 9). If the basic shot-domain noise models are summed with both the modeled data for the base-line and time-steps, they will subtract out during the 4D differencing. Therefore, randomized versions of the basic shot-domain noise models are summed with the time-step finite-difference modeled shot gathers.

To verify that the modeled gathers plus noise models accurately represents the recorded data, the datasets are calibrated using CMP variograms (Calvert, 2005). Figure 10 shows the CMP variograms for the data from Figure 8: the real data (blue) and its three components: random noise (orange), residual coherent noise (red), and real data minus the noise models (black). Figure 10 also shows the CMP variograms for the data from Figure 9: the modeled data (purple) and the modeled data plus calibrated noise models (green). The variograms of the modeled data plus calibrated noise models (green) plots through the variogram of the real data (blue), indicating the modeled data plus calibrated noise models are a reasonably accurate representation of the real data.

Finite-Difference Forward modeling and Reverse-Time Migration Imaging without Calibrated Noise (Noise Free)

By first looking at forward modeling without noise, simulated reservoir property changes can be linked to the corresponding 4D time-lapse response, in order to provide a qualitative understanding of the nature, magnitude, and distribution of the predicted 4D time-lapse response into future time.

The reservoir simulations from the Chimera DIEM are transformed into isotropic 3D petro-elastic property models Vp, Vs, and density for each time-step for forward-modeling and imaging. The master acquisition geometry and parameters used for the forward-modeling are described in Table 1. The data are forward-modeled without a free-surface, hence free-surface multiples are absent, and the direct arrival is attenuated using linear noise attenuation.

The finite-difference modeling and reverse-time migration (depth) imaging are performed with the 3D petro-elastic property models corresponding to each time-step. The base-line data are simulated by decimating the master geometry shot gathers modeled with a 50m shot line interval to a 200m shot line interval prior to imaging. Figure 11 depicts an inline, cross-line and time-slice through the noise free 3D finite-difference modeled and reverse-time migrated data for the 2014 base-line date. Figure 12 shows a vertical inline cross section for 2014, 2017 and the 4D time-lapse difference between 2017 and 2014.

Figure 13 left shows the reservoir pressure for 2014, 2017, 2020, and 2026, production begins in 2014, and the pressure declines as the reservoir depletes; water injection into the oil leg is initiated in 2017, resulting in a smaller decline in pressure from 2017 to 2020, and from 2020 to 2026 the pressure remains stable. Figure 13 right shows the oil saturation for the same time-steps, for each time-step there is an overall reduction in oil saturation with the largest reduction occurring at the top of the oil-leg as the gas-oil interface moves updip.

From 2014 to 2017 and 2017 to 2020 the pressure declines as the reservoir depletes, with the greatest pressure decline occurring from 2014 to 2017. These changes in pressure translate, via the rock-physics model, into a velocity change within the reservoir interval, as shown in the upper row of Figure 14; the lower row shows the corresponding noise free 4D time-lapse differences induced by these velocity changes.

With a change in velocity, there is a change in reflection coefficient, and a corresponding change in transmission coefficient. The velocity changes within the reservoir interval therefore results in a 4D time-lapse amplitude difference of the depth-migrated seismic data (primaries, interbed multiples etc.) within and below the reservoir as shown on the bottom row of Figure 14. As the data examples shown here are depth-migrated the 4D time-lapse response is an amplitude difference, if the data were time-migrated the corresponding difference would appear as both an amplitude difference and a time-shift. These complex wave propagation effects are beyond the comprehension of a Sim-to-Seis type workflow.

To gain a qualitative understanding of the 4D-response, the reservoir properties for each time-step are translated via the rock-physics model, into 3D petro-elastic property models of Vp and density. From which 3D acoustic impedance models can be calculated and differenced. Such that the changes in reservoir properties: pressure, oil saturation etc. are expressed as a change in acoustic impedance. By comparing the changes in acoustic impedance within the reservoir interval, with the modeled 4D time-lapse differences, seismic events visually correlating with the changes in acoustic impedance can be identified.

The upper row of Figure 15 depicts the acoustic impedance changes; the lower row, the corresponding 4D time-lapse amplitude differences plotted at the same scale. For both time-steps, there is a clear and strong visual correlation between the movement of the gas-oil interface visible on the acoustic impedance change and a seismic event, both indicated by the blue arrows. However, the movement in the oil-water interface is less obvious. For the 2020 to 2017 time-step, there is no seismic event indicated by the green arrow that correlates with movement of the oil-water interface visible on the acoustic impedance change. For the 2026 to 2020 time-step there is a tenuous visual correlation between the seismic event indicated by the green arrow and the movement of the oil-water interface visible on the acoustic impedance change.

The implication, therefore, is that the amplitude change resulting from the movement of the oil-water interface is smaller than the amplitude change caused by the transmission coefficient effect as the wave-field propagates through the reservoir. Although the acoustic impedance change is clear within the reservoir, and strongest at the gas-oil and oil-water interfaces, the collective changes within the reservoir interval result in a complex 4D time-lapse response within and below the reservoir, which partially or completely masks the 4D time-lapse response from the acoustic impedance change due to movements in the gas-oil and oil-water interfaces. This is not an effect that can be modeled and hence predicted by a Sim-to-Seis type workflow. The left image in Figure 16 shows a depth-slice through gas-oil interface, from the modeled noise-free 4D time-lapse difference for the 2014 to 2017 time-step. The right image shows the corresponding depth-slice through the acoustic impedance change, derived from the petro-elastic models. The dashed line annotated on both defines the periphery of the acoustic impedance change. The acoustic impedance change maps the spatial distribution and magnitude of the 4D-response predicted by the reservoir simulation. The modeled noise-free 4D time-lapse difference shows how the acoustic impedance change is recorded by time-lapse seismic with a specific acquisition geometry when illuminated through, and distorted by, a specific overburden and near surface model. Hence, in would be misleading to interpret the differences between the acoustic impedance change predicted by the reservoir simulation and the 4D time-lapse acoustic impedance difference derived via inversion of the 4D time-lapse amplitudes, as a function of a reservoir property change due to production.

Finite-difference modeling and reverse-time (depth) migration imaging without survey specific calibrated noise connects simulated reservoir property changes to the corresponding 4D time-lapse seismic response, providing a qualitative understanding of the nature, magnitude and distribution of the predicted 4D time-lapse seismic response into future time. However, it does not determine if the 4D-respose will be measurable with the inherent residual noise conditions associated with the acquisition and processing of 4D time-lapse seismic data.

Finite-Difference Modeling and Reverse-Time (Fepth) Migration Imaging with a Calibrated Noise Model

To determine if the 4D-respose will be seismically measurable, representative noise models are required. The measured base-line seismic data immediately prior to the imaging step is an ideal dataset for noise model derivation. At this stage in the processing of the base-line data all signal processing, data conditioning, multiple attenuation and noise attenuation etc. have been performed and the resultant data comprises seismic signal, residual coherent noise and random noise, from which the residual coherent noise and random noise models can be decomposed (Figure 8). The resultant noise models are scaled and summed with the finite-difference modeled shot gathers (Figure 9), and to ensure that the shot gathers with noise models are a reasonably accurate representation of the real data, they are calibrated using CMP variograms (Figure10). Once calibrated, the modeled shot gathers with noise are imaged and the images differenced to generate the modeled 4D time-lapse difference with calibrated noise.

Figure 17 shows the modeled noise-free 4D time-lapse differences for four time-steps, which chart the evolution of the 4D-respose associated with gas-oil interface and oil-water interface from 2014 to 2038. The 4D time-lapse response for the time intervals from 2020 are lower amplitude than for the interval 2014 to 2017, for they have been differentially scaled for presentation purposes.

Figure 18 shows the modeled 4D time-lapse differences with calibrated noise for the same four time-steps as Figure 17. What is evident from Figure 18 is that the 4D-respose associated with gas-oil interface and oil-water interface are no longer visible for any time-step. Hence, we can conclude that the 4D-respose will not be measurable with the base-line acquisition geometry, with its 200m shot line interval, and the inherent survey specific residual noise resulting from the processing sequence applied to the measured base-line seismic data

Given that the 4D-respose is unmeasurable with the base-line acquisition geometry, after the inclusion of calibrated residual noise, there are two obvious courses of investigation. The first is the processing sequence applied to the base-line dataset from which the noise models were derived. Can a more rigorous and robust processing sequence be designed to minimize the residual coherent and random noise remaining in the data prior to the imaging step? If so new survey specific noise models can be built, calibrated, and the imaging part of the modeling workflow repeated. The alternative option is to reduce the shot-line interval from the base-line spacing of 200m. Given the master geometry shot-line interval used for finite-difference modeling was 50m, no additional modeling is required. The master geometry can be decimated to alternative shot-line intervals less that 200m and the calibrated noise and imaging part of the modeling workflow repeated.

If neither option delivers a measurable 4D-response, then alternative measurement methods should be considered: 3D VSP, cross-well measurements etc. all can be modeled using a variation of the above workflow.

Once a measurement method and appropriate geometry have been determined, the sensitivity of the 4D-response to uncertainties in the reservoir model, rock physics model, and acquisition positional errors etc. can be studied by repeating the workflow with the appropriate variation.

Conclusion

One component of the redefined closed-loop seismic reservoir monitoring workflow is Full-Field 4D Image-Modeling. Full-field 4D image-modeling incorporates the geologic, reservoir simulation, and reservoir geomechanical models into an integrated full-field coupled dynamic integrated earth model to surface, from which 3D grids of petro-elastic parameters for a range of reservoir simulations are derived via the rock-physics model for input into finite-difference forward-modeling and imaging. By including 3D wave propagation, acquisition geometry, overburden illumination, near surface effects and calibrated noise the seismically measurable 4D-response predicted via full-field 4D image-modeling is more robust, and of a higher fidelity than is achievable via the more traditional Sim-to-Seis type workflows.

Full-Field 4D Image-Modeling workflow:

- Integrates the reservoir, geologic and geomechanical models into a dynamic integrated earth model, from which all aspects of the 4D-response, time-shifts, amplitude changes, AVO changes, compaction and subsidence to surface can modeled into future time for a range of production scenarios.
- Noise free forward-modeling provides a qualitative understanding of the nature, magnitude and distribution of the 4D-response into future time and ties reservoir changes to the corresponding seismically measurable 4D-response.
- With the inclusion of calibrated noise the forward-modeling models the seismically measurable 4D-response, from which the optimal measurement method and acquisition design can be determined to record the seismically measurable 4D-response at the required time-steps for proactive seismic reservoir monitoring.
- Moreover, with the advent of modern compute architectures the elapsed time for the full-field 4D image-modeling is measured in single digit months.

Full-Field 4D Image-Modeling is necessary to fully understand the complexities of reservoir property changes over time, to assess whether those changes are seismically detectable, and to make informed decisions on the 4D time-lapse measurement method, design, and reservoir monitoring strategy. Such an in-depth understanding cannot be achieved using one of the more traditional Sim-to-Seis type workflows.

Selected References

Calvert, R., 2005, Insights and methods for 4D reservoir monitoring and characterization: SEG Distinguished Instructor Series No. 8.

Gosselin, O., S.I. Aanonsen, I. Aavatsmark, A. Cominelli, R. Gonard, M. Kolasinski, and K. Neylon, 2003, History matching using time-lapse deismic (HUTS): SPE paper 84464.

Hurren, C.A., C. Broad, G. Duncan, R.A. Hill, and D.E. Lumley, 2012, Successful application of 4D seismic in the Stybarrow field, Western Australia: SPE-158753-MS. Website accessed October 16, 2016, https://www.onepetro.org/conference-paper/SPE-158753-MS.

Johnston, D.H., 2013, Practical applications of time-lapse seismic data: SEG Distinguished Instructor Series No. 16.

Lecomte, I., H. Gjøystdal, Å. Drottning, F.A. Maaø, T.A. Johansen, and R. Bakke, 2004, Efficient and flexible seismic modeling of reservoirs: A hybrid approach: The Leading Edge, v. 23/5, p. 432-437.

Pluchery, E., S. Toinet, P. Cruz, A. Camoin, and and J. Franco, 2013, Intensive use of 4D seismic in reservoir monitoring, modeling and management: The Dalia case study: International Petroleum Technology Conference, IPTC 17047, p. 4725-4730.

Rabani, M.N.A., E. Adams, A. Ryba, J. Harwijanto, G. Warrlich, L.H. Fui, and W. Van Zandvoord, 2014, An integrated approach to understand the remaining potential and ultimate hydrocarbon recovery of a giant carbonate gas field, Offshore Sarawak, Malaysia:. Offshore Technology Conference. OTC-24994-MS. Website accessed October 16, 2016, https://www.onepetro.org/conference-paper/OTC-24994-MS.

Taggart, I., A. Ali, B. Mee, M. Smith, A. Gerhardt, and L. Bourdon, 2008, Integrating 4D seismic data with production related effects at Enfield, North West Shelf, Australia:. Society of Petroleum Engineers, SPE-116916-MS. Website accessed October 16, 2016, https://www.onepetro.org/conference-paper/SPE-116916-MS.

Ullmann De Brito, D., Caletti, L., and Moraes, R. [2011], Incorporation of 4D seismic in the reconstruction and history matching of Marlim Sul Deep Water Field flow simulation model: Society of Petroleum Engineers, SPE-143048-MS. Website accessed October 16, 2016, https://www.onepetro.org/conference-paper/SPE-143048-MS.

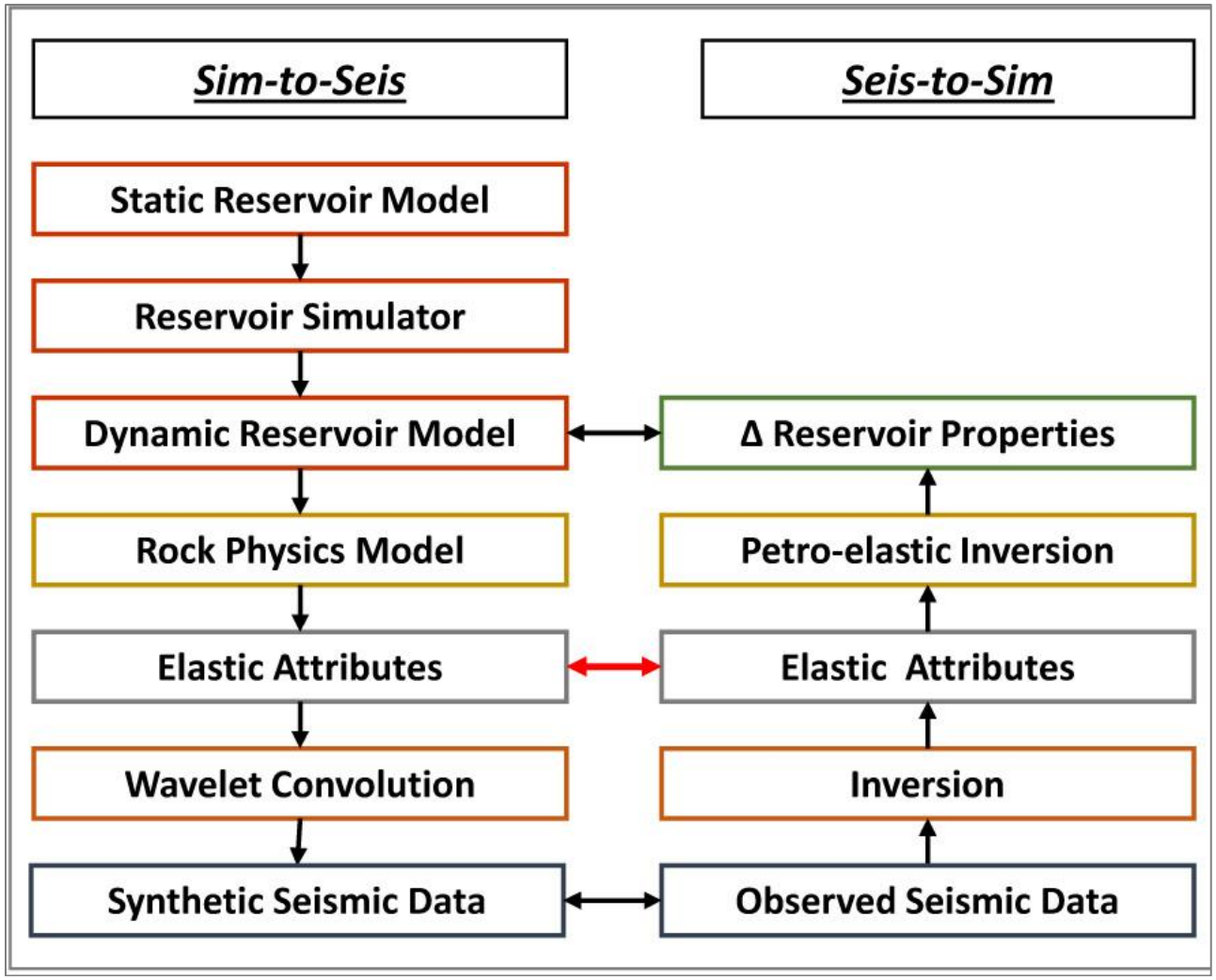

Figure 1. Example Sim-to-Seis and Seis-to-Sim workflows.

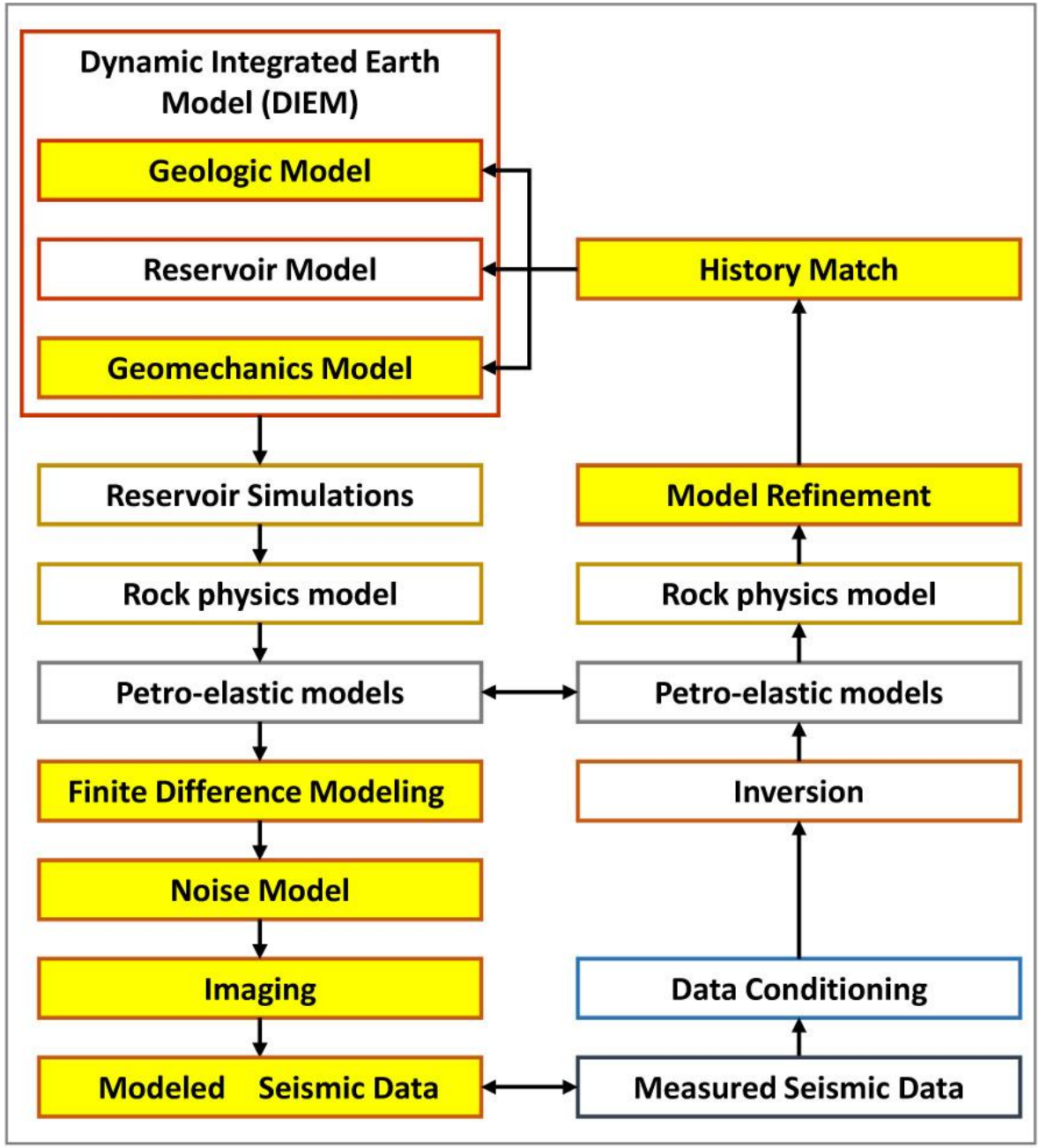

Figure 2. A redefined CL-SRM workflow; white boxes as HUTS and yellow boxes redefined additions.

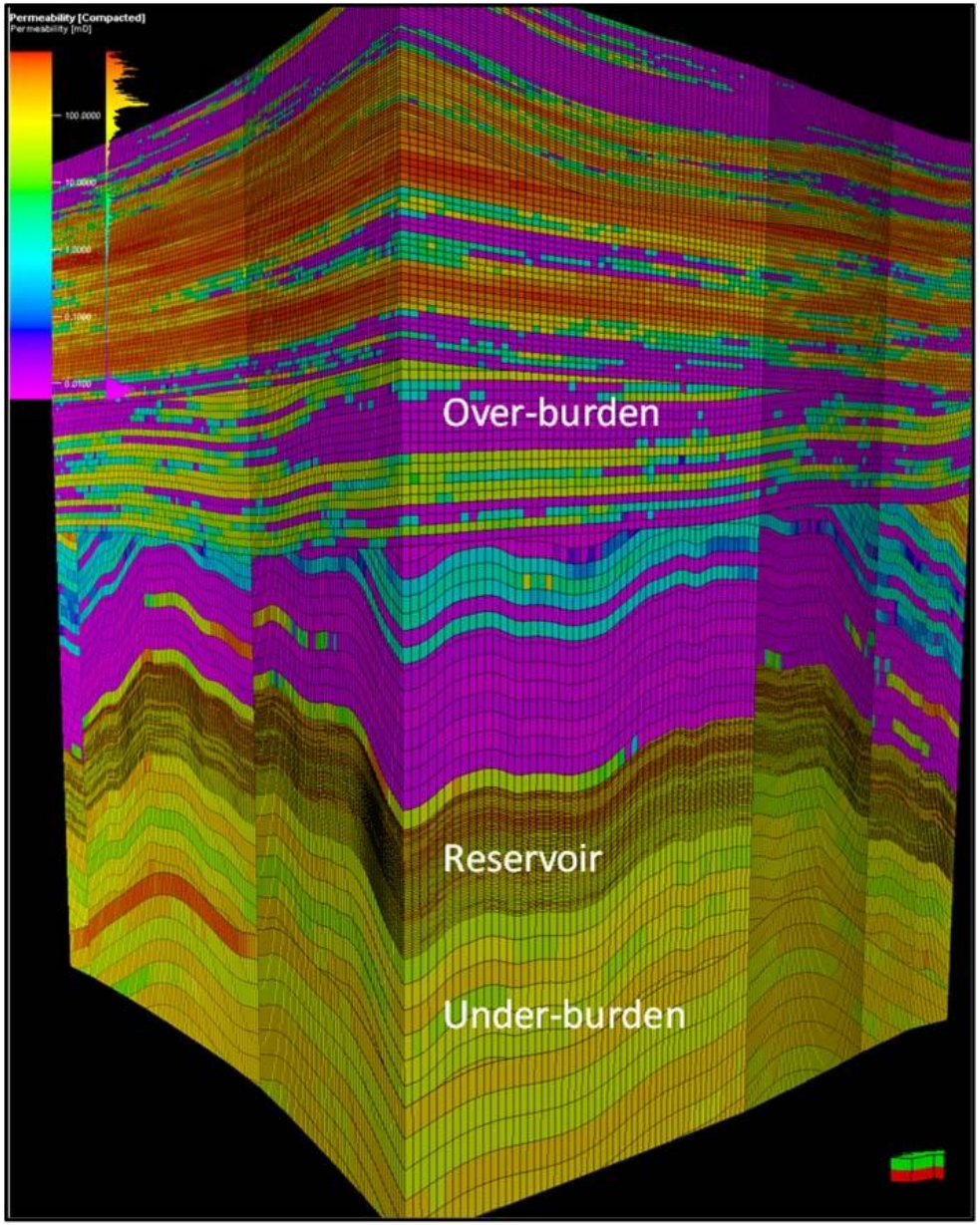

Figure 3. Chimera DIEM.

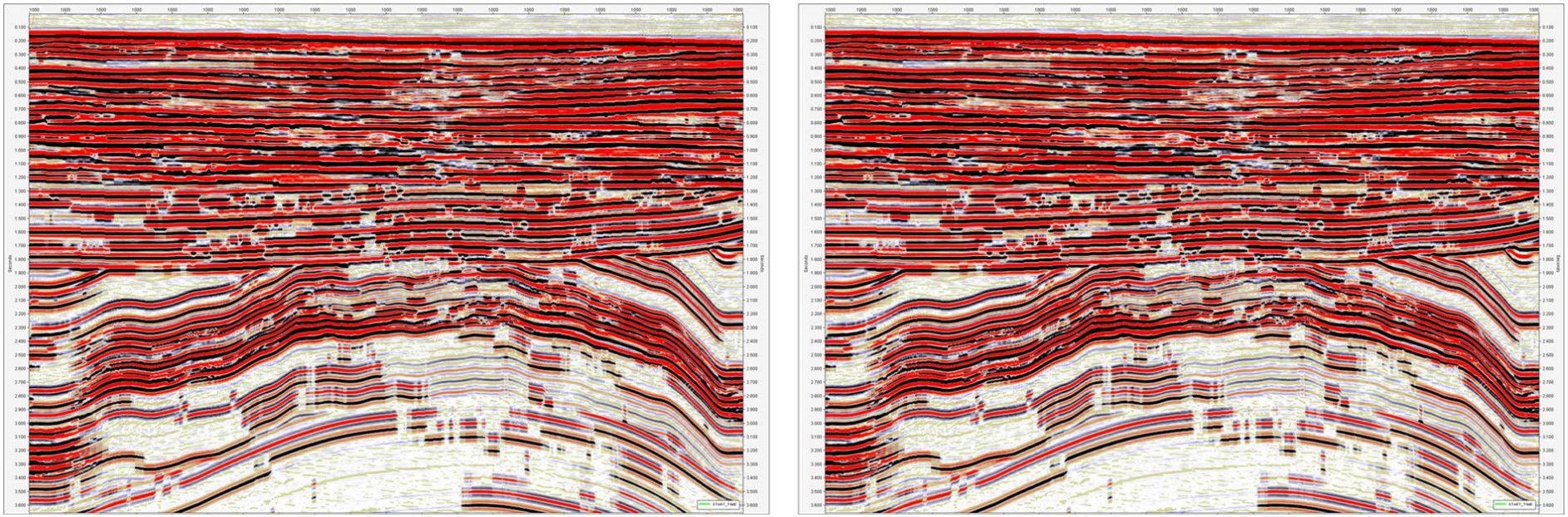

Figure 4. Reflectivity: 3D 30hz Ricker point spread function. Left 2014; right 2017.

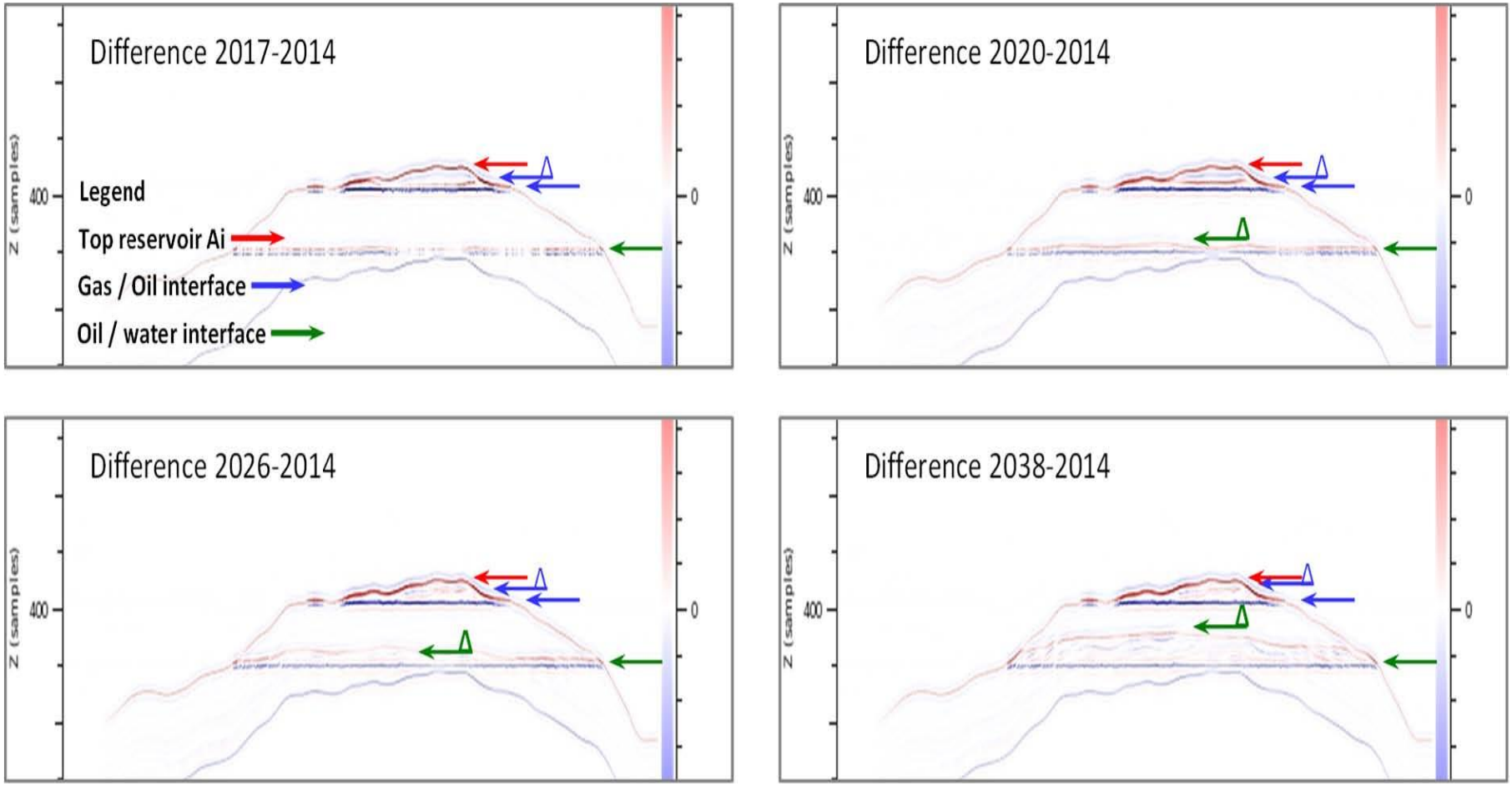

Figure 5. Point spread function 4D time-lapse differences for 2017 to 2014, 2020 to 2014, 2026 to 2014 and 2038 to 2014.

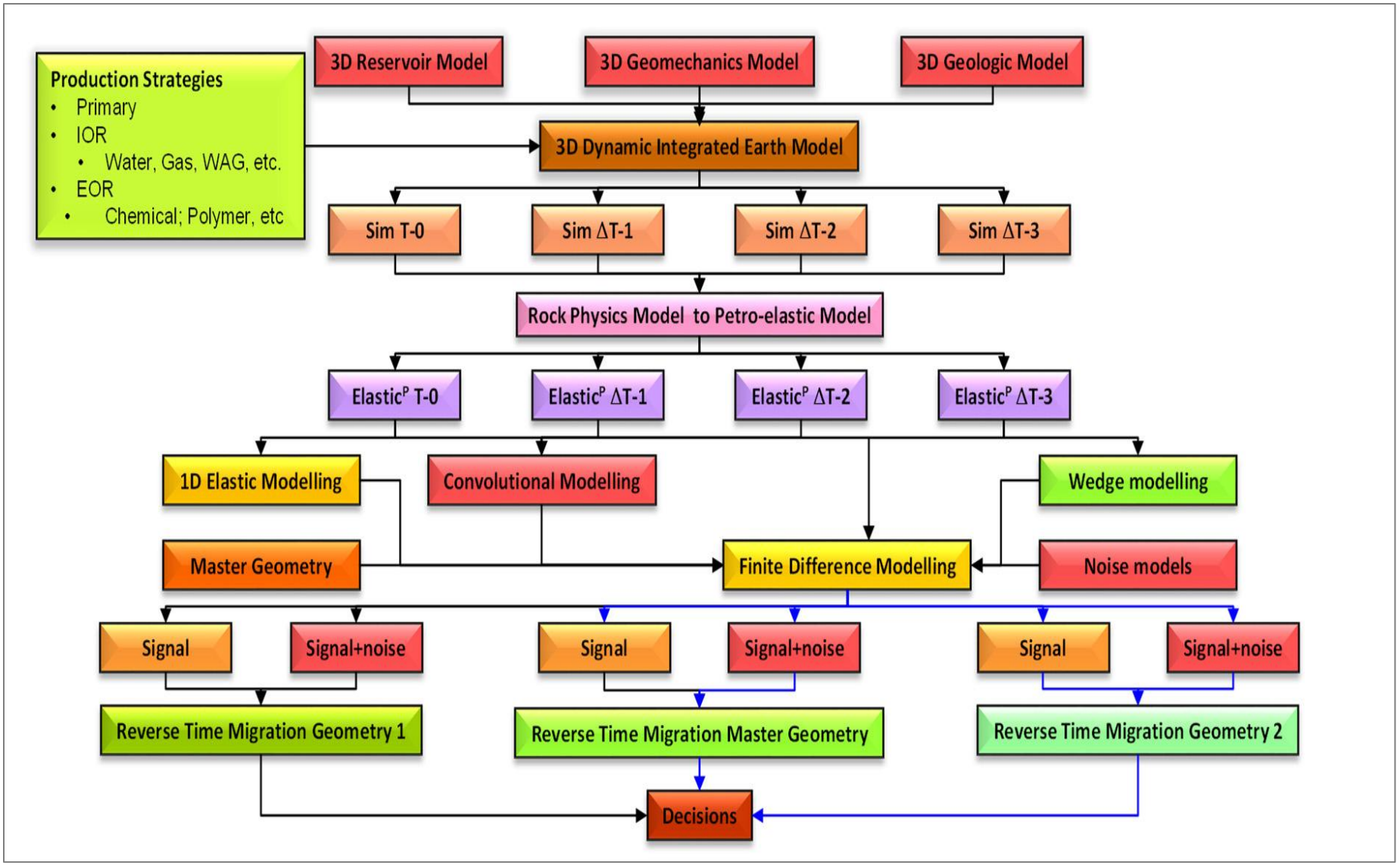

Figure 6. A robust full-field 4D image modeling workflow; back arrows identify primary path; blue arrows, a conditional path.

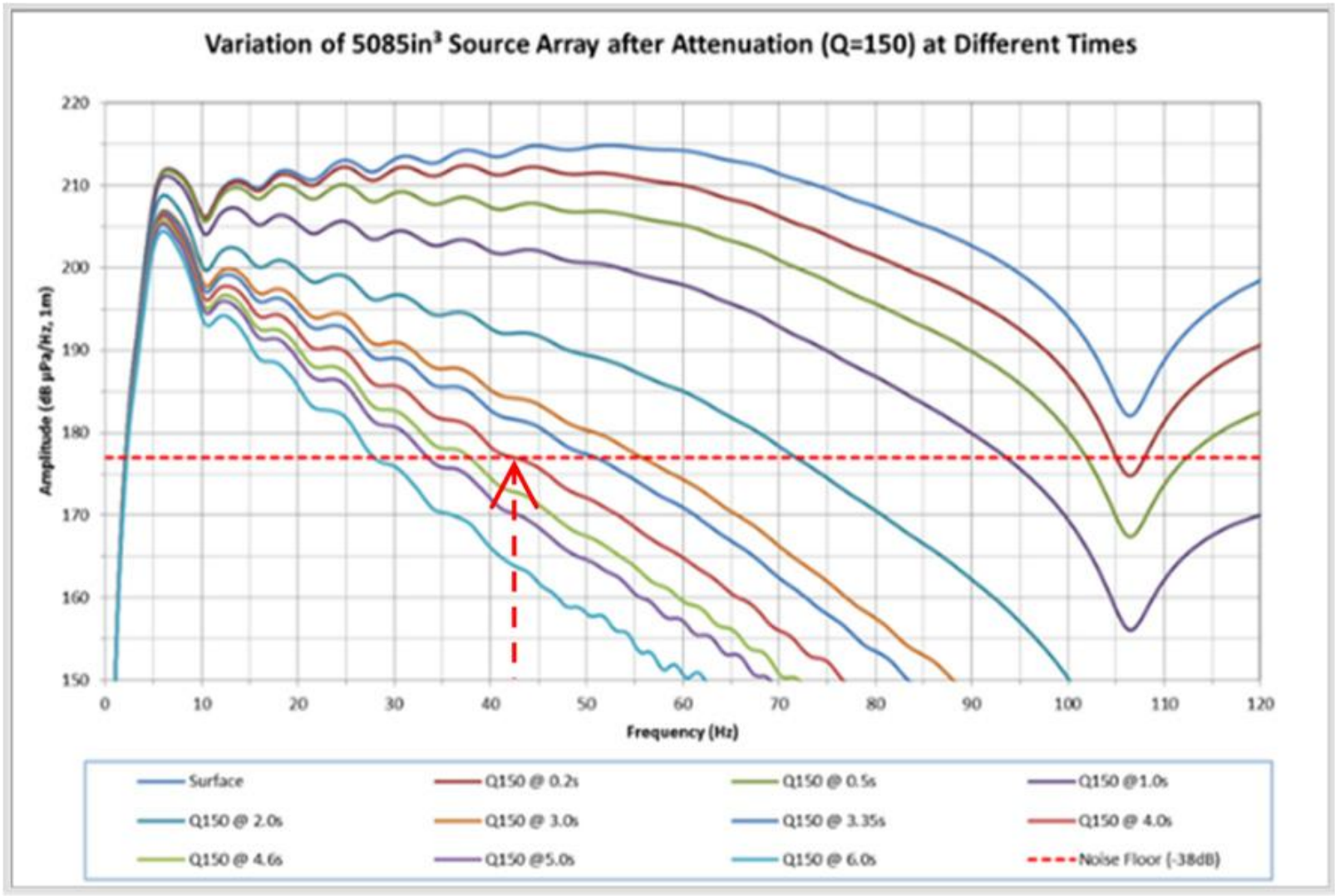

Figure 7. Amplitude spectra for a 5085 cu in source array, as a function of two-way traveltime.

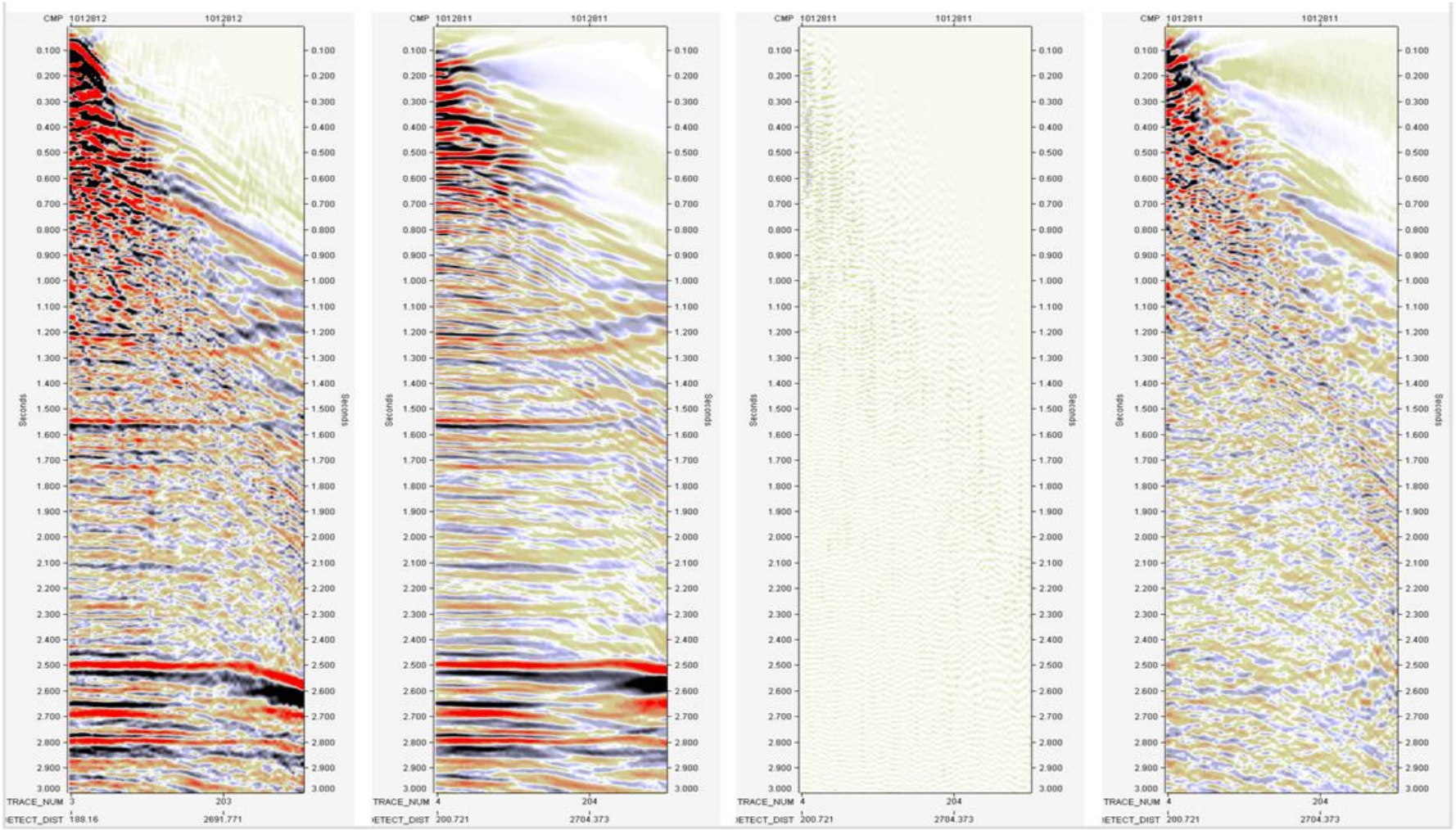

Figure 8. Left to right: 1) CMP gather prior to pre-stack imaging; 2) after random and residual coherent noise removal; 3) random noise model; 4) residual coherent noise model.

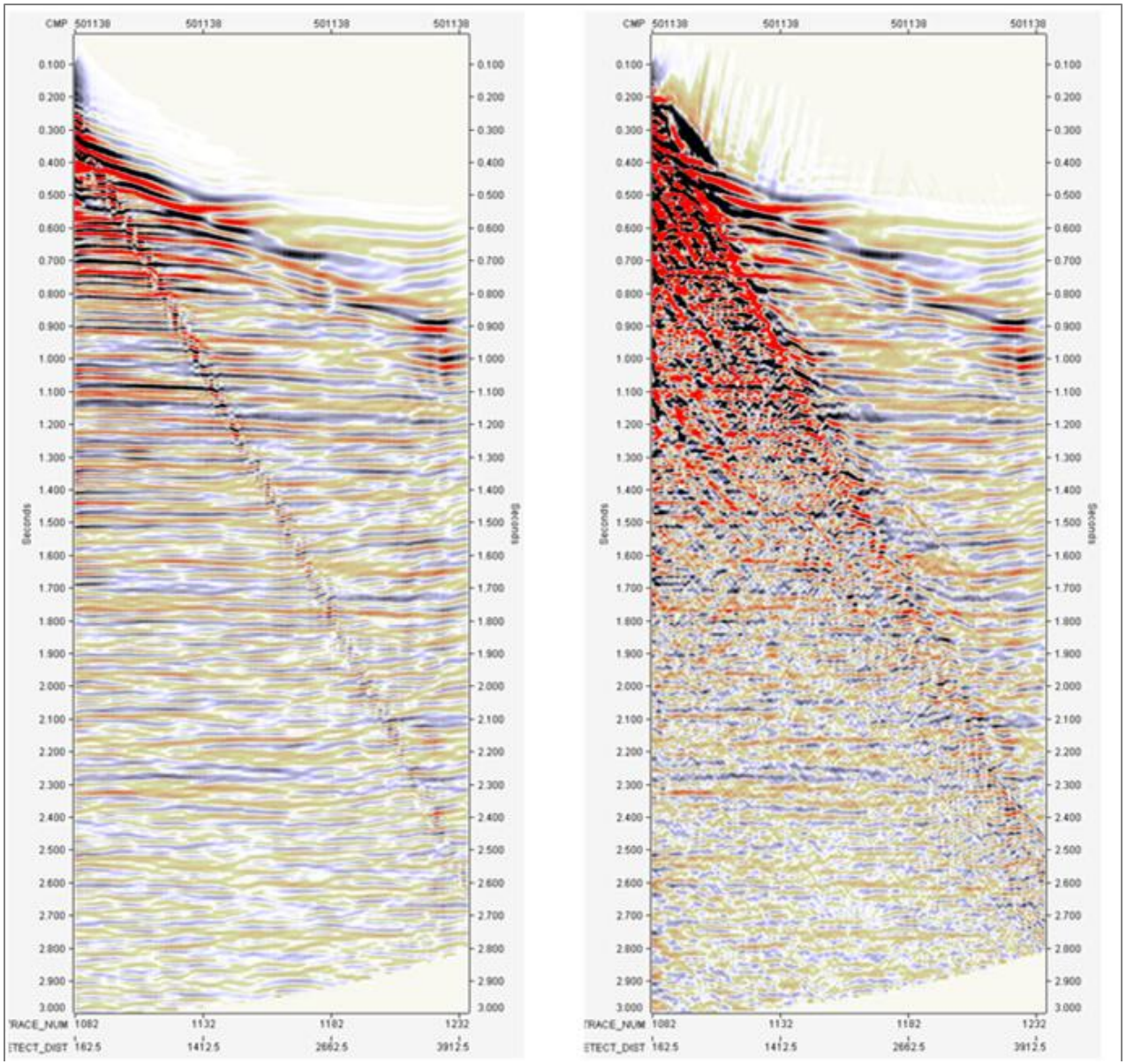

Figure-9. Left - Finite difference modeled shot gather, Right – with scaled and calibrated noise models.

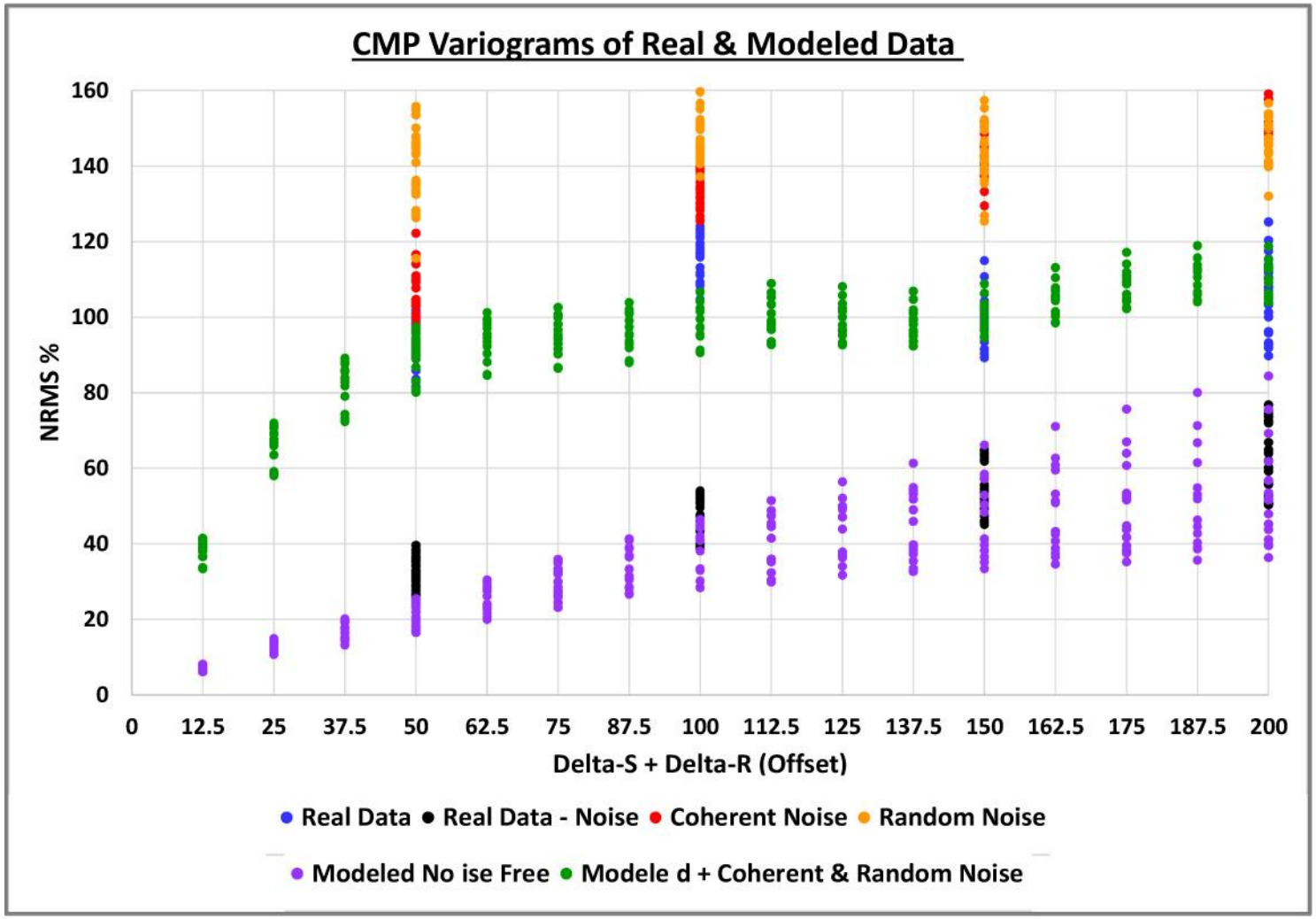

Figure 10. CMP variogram derived from the real and modeled data.

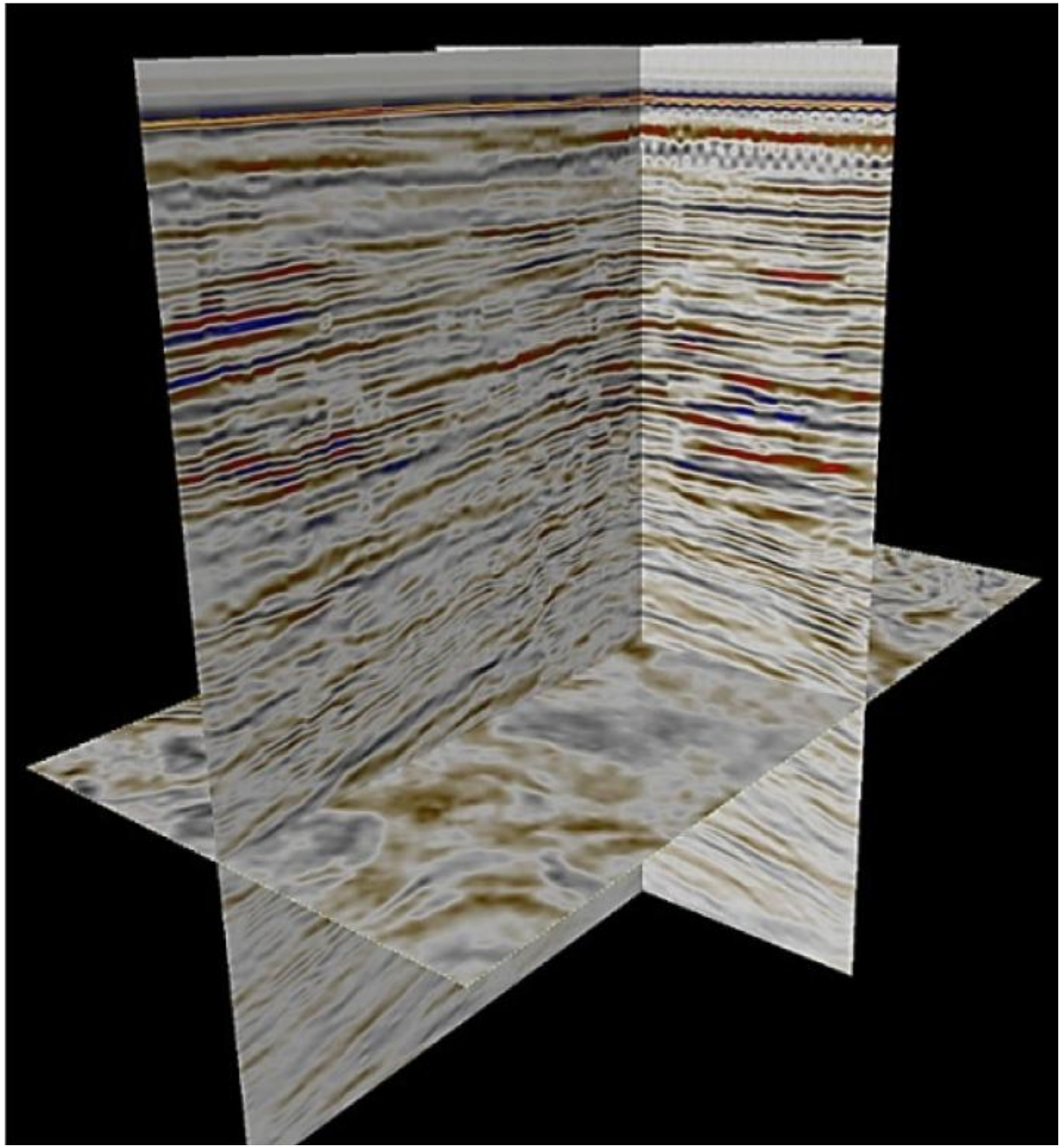

Figure 11. Noise free forward-modeled and imaged 2014 base-line data in depth.

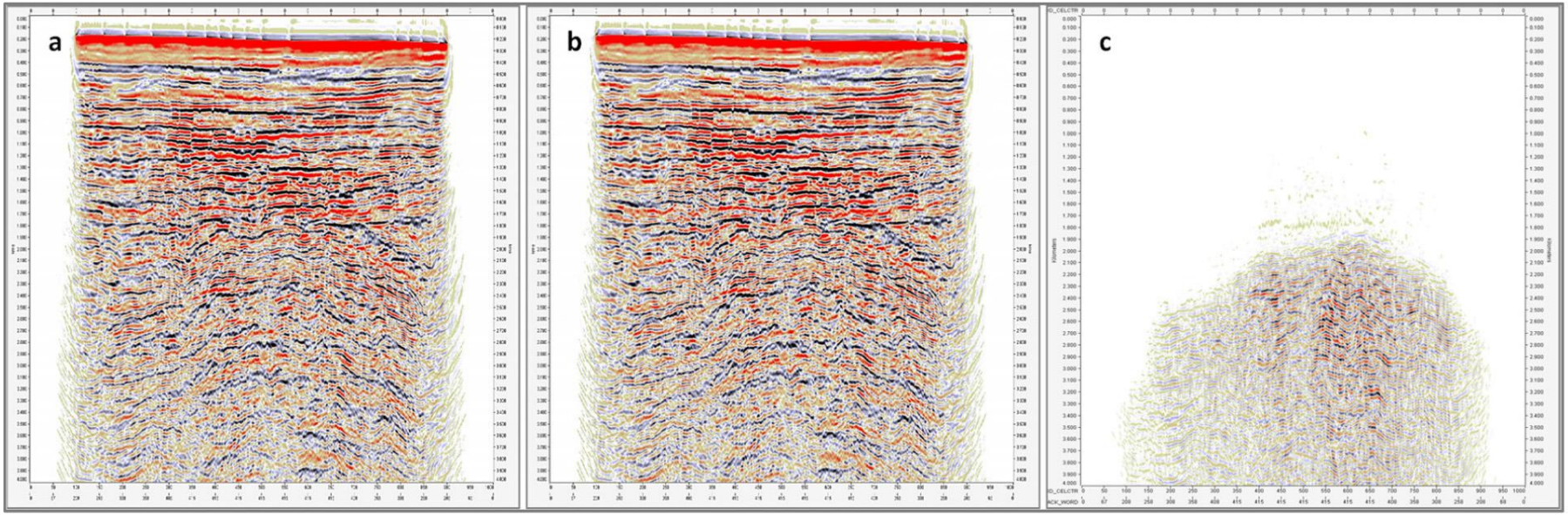

Figure 12. Noise free 3D finite difference modeled and reverse time migrated data: a. 2014 inline, b. 2017 inline, c. the 4D time-lapse difference - 2017 minus 2014.

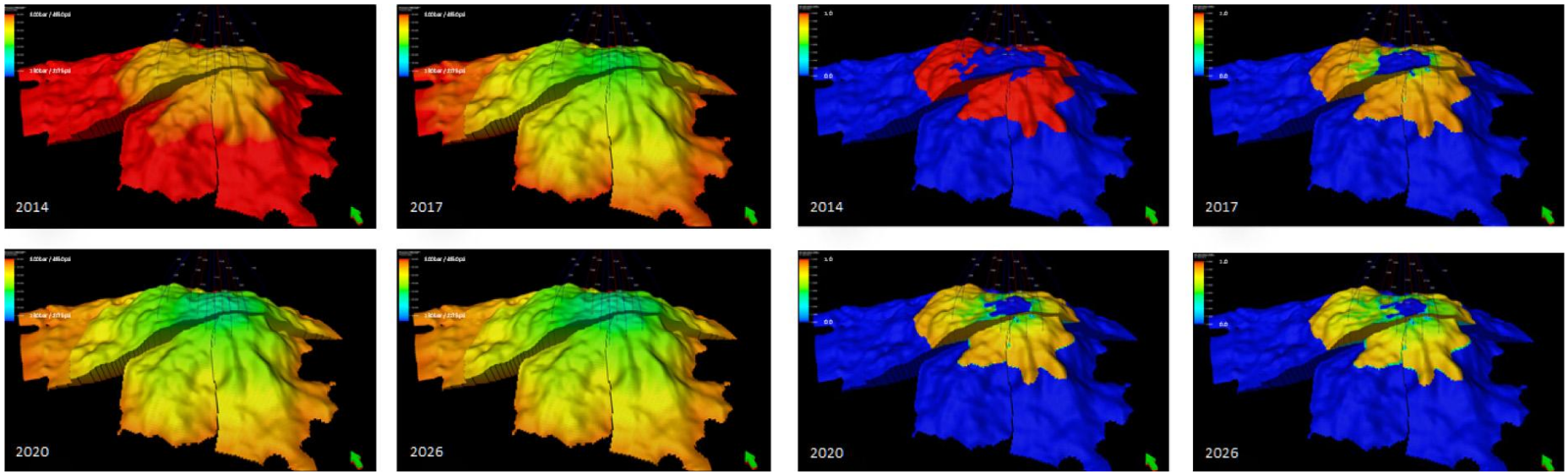

Figure 13. Left - Reservoir pressure from 2014 to 2026. Right - Reservoir oil saturation for the same time-steps.

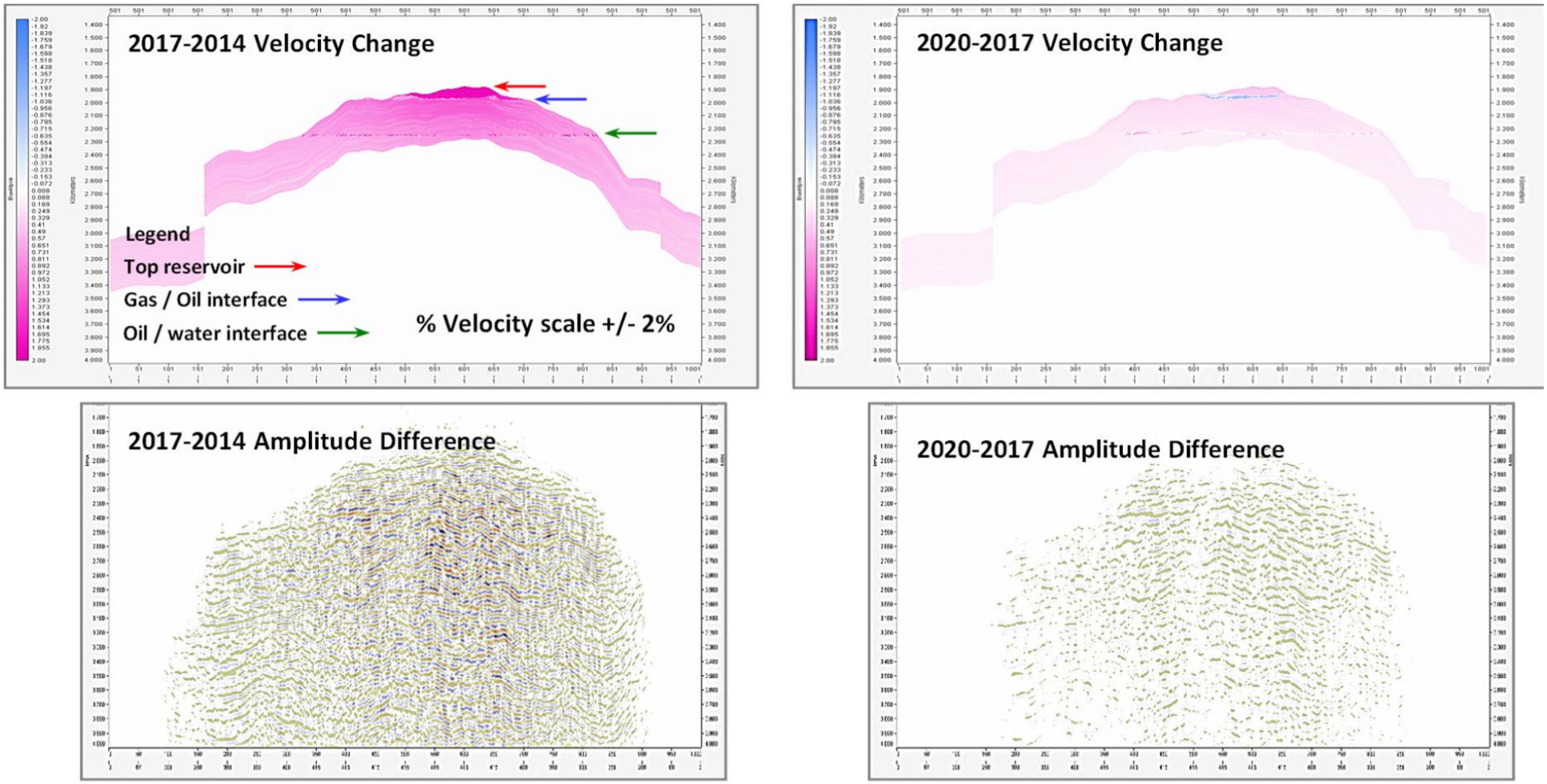

Figure 14. Upper row - the velocity changes within the reservoir interval implied by the corresponding pressure changes illustrated in Figure 13 left. Lower row - the 4D time-lapse amplitude difference induced by the velocity changes within the reservoir interval.

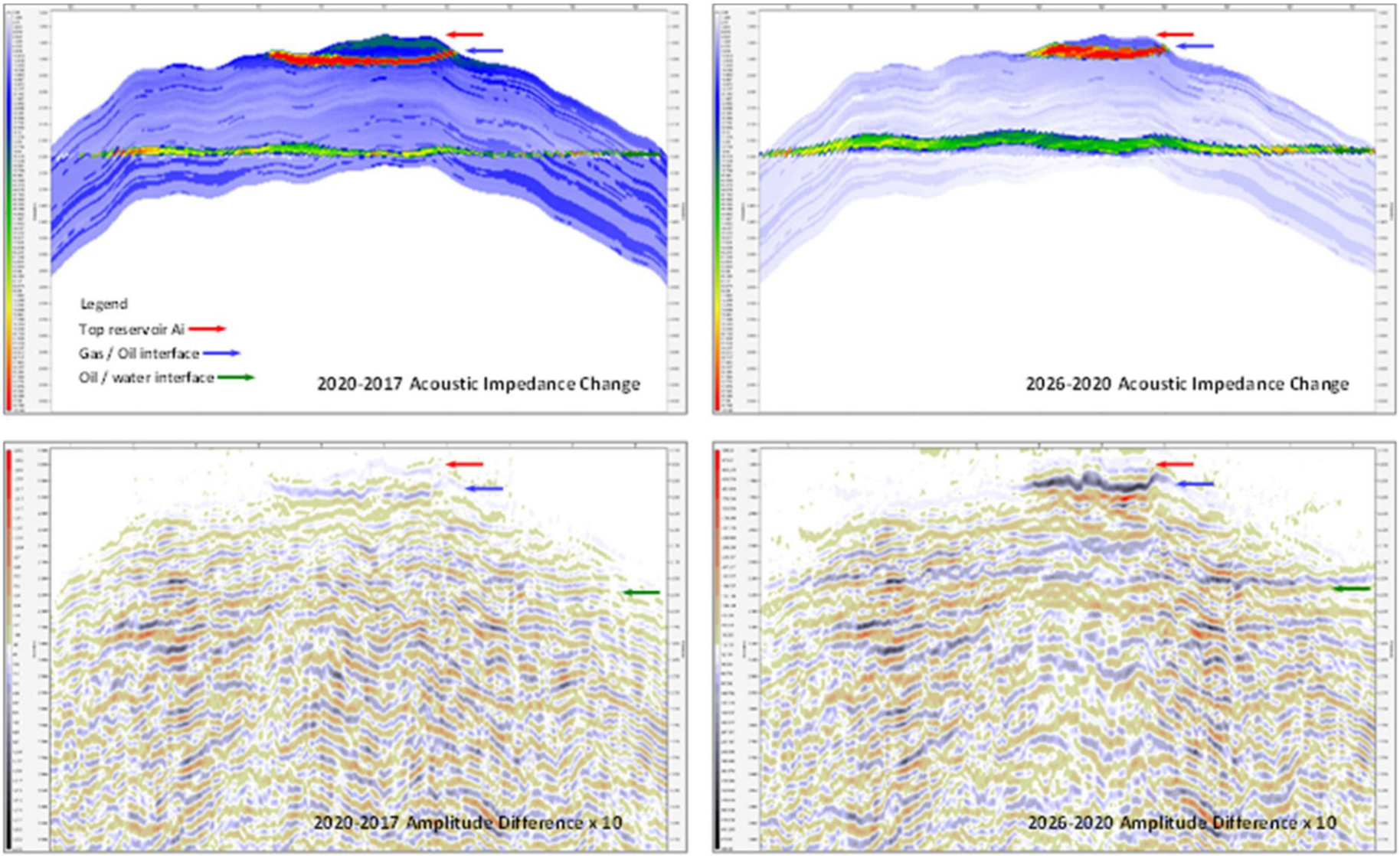

Figure 15. Upper row - 4D time-lapse changes in acoustic impedance for time-steps 2020-2017 and 2026-2020. Lower row – 4D time-lapse amplitude difference for time-steps 2020-2017 and 2026-2020 (Amplitude differences are scaled x 10).

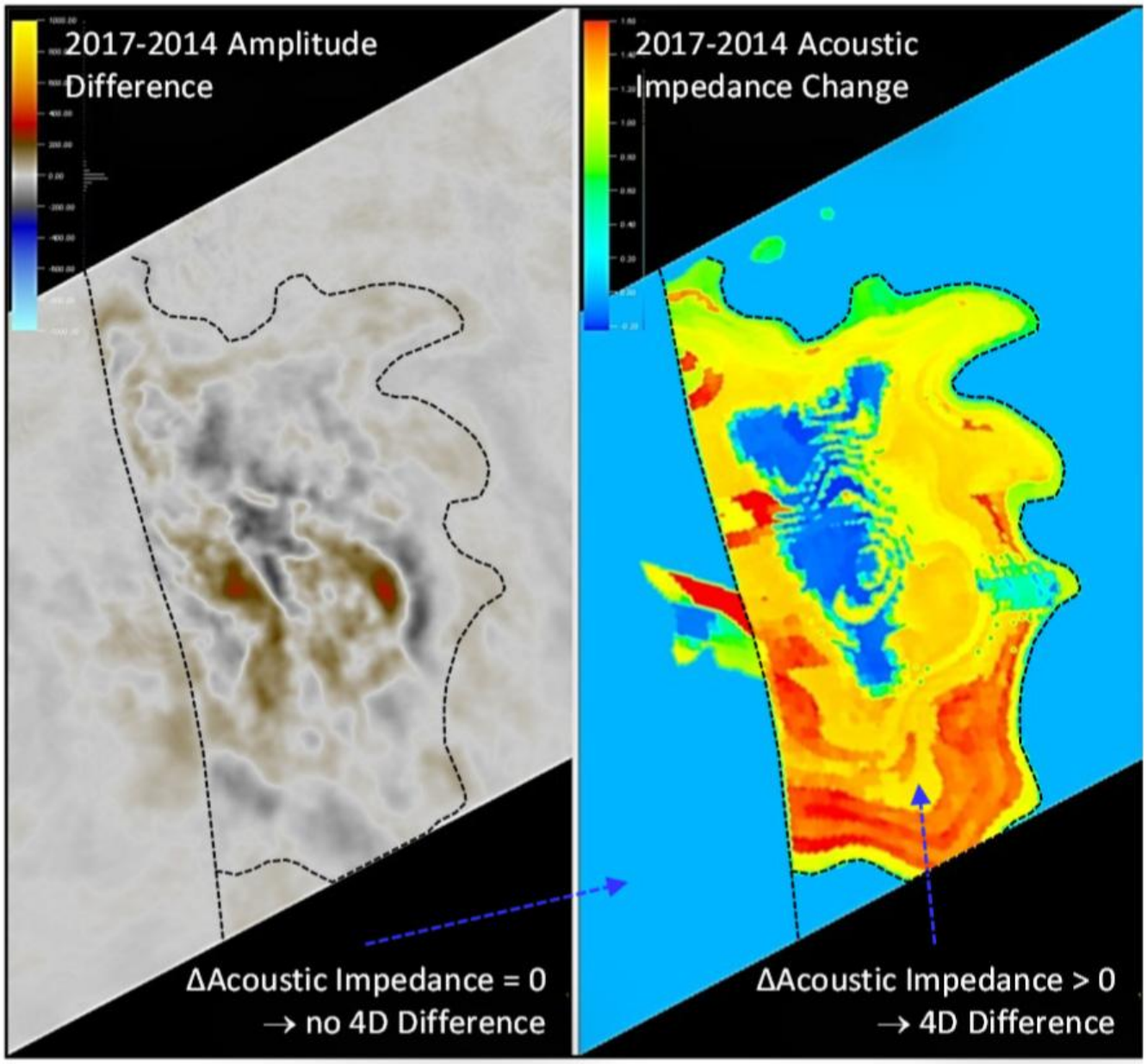

Figure 16. Depth-slices of amplitude difference and acoustic impedance change.

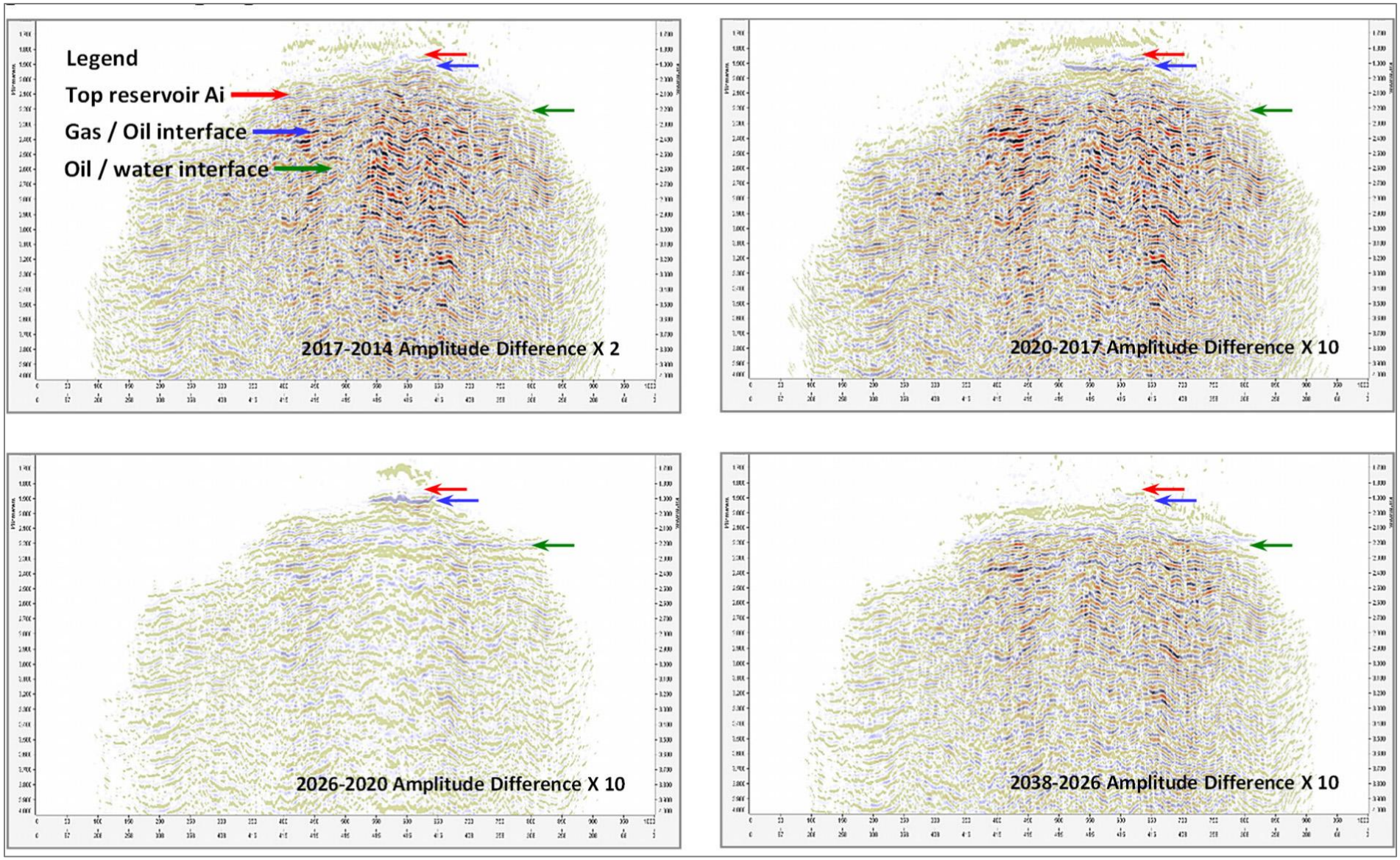

Figure 17. Modeled noise-free 4D time-lapse differences for time-steps: 2017-2014, 2020-2017, 2026-2020, and 2038-2026.

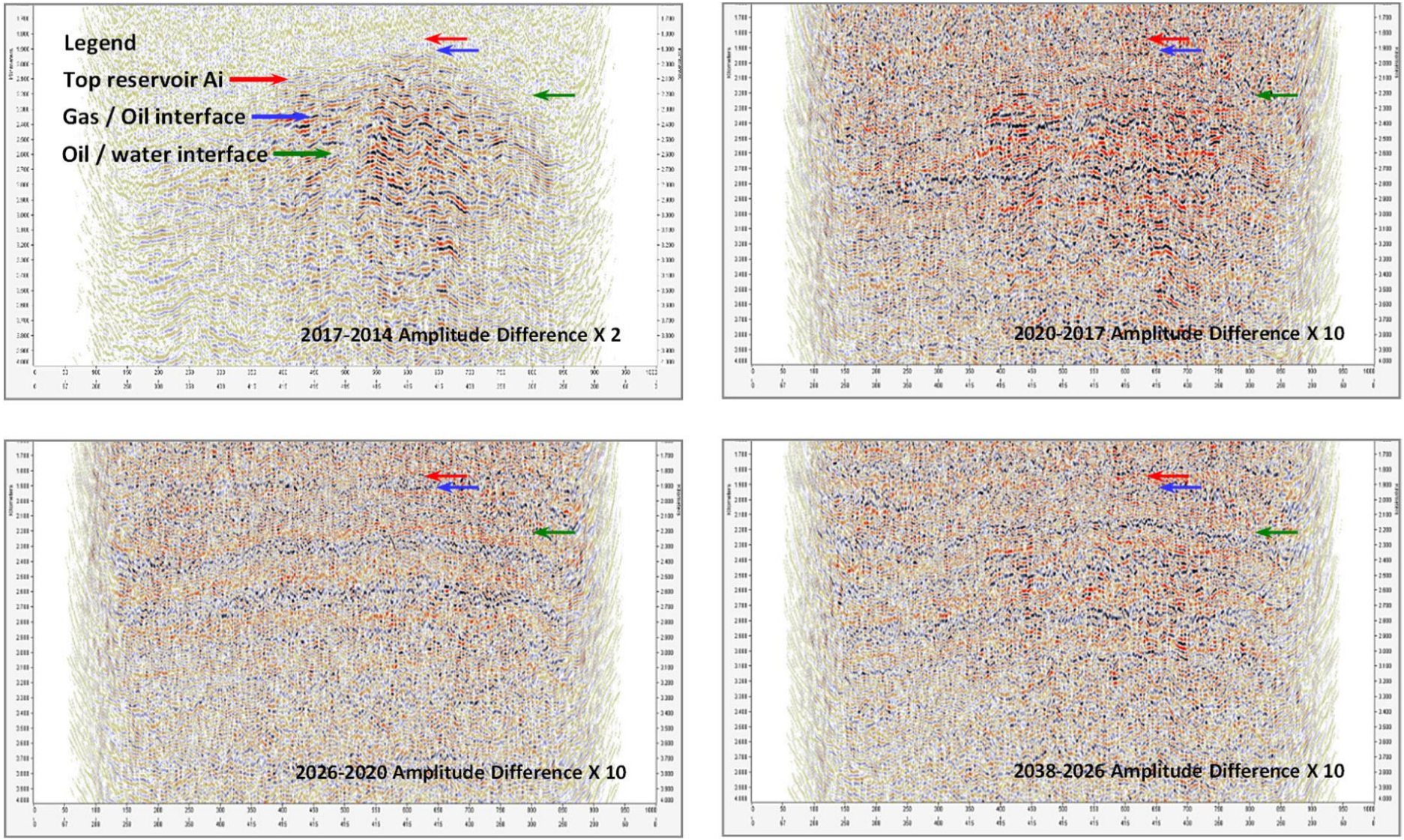

Figure 18. Modeled 4D time-lapse differences with calibrated noise for time-steps: 2017-2014, 2020-2017, 2026-2020, and 2038-2026.

Table I: Master acquisition geometry	
Source array	5085 cu in airgun
• Depth	6m
• Shot point interval	25m
• Shot line interval	50m
Receiver Array	Square: center source
• Depth	200m (Sea bed)
• Maximum inline offset	4000m
• Maximum crossline offset	4000m
• Receiver spacing	12.5m x 12.5m
Modeling bandwidth	Up to 60hz

Table 1. Master acquisition geometry.